On the density structure of far-wake vortices in a stratified fluid

Marion Bonnier [a,b,*], Olivier Eiff [b], Philippe Bonneton [c]

[a] *Institut de Mécanique des Fluides, allée du Professeur Camille Soula, 31400 Toulouse, France*
[b] *Centre National de Recherches Météorologiques, 42 avenue G. Coriolis, 31057 Toulouse, France*
[c] *Département de Géologie et d'Océanographie, Université Bordeaux 1, avenue des facultés, Bordeaux, France*

Abstract

An experimental investigation of the three-dimensional density structure of far-wake vortices generated by moving a sphere in a linear saline stratification has been carried out via conductivity measurements. These measurements were performed in the vortex cores along vertical and horizontal profiles to capture the three-dimensional nature of the vortices. We first present a simple model of an isolated vortex, the calculated internal density field of which has been confirmed by the conductivity measurements performed in both turbulent and laminar wakes. The time-dependent density structure is also described, as well as the decay of the density peak within the vortices. An identical density structure corresponding to an intensification of the background stratification has been identified for far-wake vortices originating from either laminar or turbulent near-wakes. This suggests that these vortices exhibit universal features of quasi two-component structures in stratified fluids, such as large-scale vortices commonly found in the ocean. © 2000 Elsevier Science B.V. All rights reserved.

Keywords: Stratified fluid; Far-wake; Three-dimensional characteristics; Density measurements

1. Introduction

Turbulent motions are known to be strongly modified when subject to the constraints of a stratified medium. In its initial stage, freely decaying turbulence in stratified flows

---

* Corresponding author. Institut de Mécanique des Fluides, allée du Professeur Camille Soula, 31400 Toulouse, France. Fax: +33-5-61-07-95-66; E-mail: bonnier@cnrm.meteo.fr

behaves similarly as in a homogeneous fluid, i.e., with three-dimensional characteristics. Eventually, however, the stratification inhibits the vertical movements and the turbulence becomes highly anisotropic. During this collapse, the vortical motions loose their vertical velocity component, leading to flow dominated by the horizontal motions of quasi-steady vortices. This ultimate stage is often referred to as quasi two-dimensional turbulence, although the term quasi two-component, as first suggested by Godeferd and Cambon (1994), seems more appropriate since the associated structures are not uniform along the vertical direction but have a negligible vertical velocity component compared with the horizontal velocity component. The description of the vortices in terms of ''pancakes'' is also somewhat misleading, since they are not really as thin as the term implies.

There have been numerous studies that addressed the vertical structure of vortices in stratified media. Fundamental studies focusing on dipoles, monopoles or wakes have been undertaken both experimentally (e.g., Chomaz et al. (1993); Flór and Van Hejst (1996) or Spedding et al. (1996)), and numerically (e.g., Fung and Chang (1996)). Field studies in the ocean, on the other hand, usually examine submesoscale vortices such as meddies or gulfstream rings (e.g., McWilliams (1985)). In both types of studies, a high degree of coherence and relative stability was found to characterize the vortices. The studies also suggest that the ultimate form of vortices resulting from the relaxation of any kind of turbulent patch generated in stratified fluid is a combination of monopoles or dipoles. This apparent universality together with the coherence and stability of these vortices must be related to their three-dimensional internal structure, in which the density field plays an important role.

Several laboratory studies have given a density description of the vortices, for example, Voropaev et al. (1991) and Voropaev et al. (1997) for dipoles and monopoles, and Folkard et al. (1997) for an oscillating grid. These studies provide density profiles measured in the early stages of evolution, i.e., before the collapse of the three-dimensional initial turbulence. The profiles exhibit local mixing before the collapse occurs. Unfortunately, these laboratory studies have not examined the late evolutionary times when the vertical movements have become negligible. The internal density structure of late-time vortices has only been reported in field studies where it was also found to be characterized by a homogeneous core (Armi et al. (1989)). However, the density measurements were only made in anticyclonic vortices, which are likely to have a different structure than cyclonic vortices or late vortices in the non-rotating case. We will therefore examine the density structure of late vortices in stratified fluids and explain how the fluid adapts to form these ultimate quasi-steady vortices. These late vortices, or post-collapse vortices, are still in the weakly nonlinear regime as studied theoretically by Riley et al. (1981).

In this study, quasi two-component vortices were generated by towing a sphere in a linearly salt-stratified water tank. The governing parameters defining the regime of this flow are the Froude number, $F = U/NR$ and the Reynolds number, $Re = U2R/\nu$, where U is the sphere velocity, R is the sphere radius, N is the Brunt–Väisälä frequency defined as $N = ((-g/\rho_o)(\partial\rho/\partial z))^{1/2}$ (where ρ_o is the mean density), and ν is the kinematic viscosity. The Froude number appears to be the dominant parameter of the flow since, at least in the (F, Re) range commonly investigated in laboratory

experiments, there is only a weak dependence on the Re number (e.g., Lin et al. (1992), or Chomaz et al. (1993)). The density structure of the vortices is measured for two distinct regimes: $F = 0.4$ ($Re = 600$), corresponding to the laminar regime which is referred to as the single layer regular (SLR) regime in Chomaz et al. (1993), and $F = 6$ ($Re = 9000$), corresponding to the turbulent regime referred to as the multi-layers irregular (MLI) regime. It should be noted that $F = 6$ ($Re = 9000$) in the MLI regime is close to the single layer irregular (SLI) regime for which only one layer is present. In the turbulent regimes (SLI and MLI), the wake initially develops as it does in the non-stratified case before collapsing into a quasi two-component Kármán-like vortex street with a negligible vertical velocity component. In the laminar regime (SLR), the wake immediately develops into a quasi two-component Kármán-like vortex street: the fluid does not have enough potential energy to pass over the sphere and therefore passes around the sphere generating vertical vorticity. The study of those two regimes thus provides a convenient way to compare the density structure of quasi two-component vortices with different mechanisms of generation.

After presenting the experimental details in Section 2, a theoretical description of far-wake vortices will be proposed in Section 3, yielding the expected density structure. This density structure will be experimentally confirmed for laminar and turbulent wakes in Section 4 and the results and implications will be discussed in Section 5.

2. Experimental set-up

The experiments were carried out in a rectangular tank ($0.7 \times 0.8 \times 7$ m^3) (Fig. 1) at the Centre National de Recherches Météorologiques in Toulouse. The quasi two-component vortices were experimentally generated by towing a sphere of radius $R = 5$ cm in a linear saline stratification of Brunt–Väisälä frequency around 1 rad/s corresponding to a variation of about 1.4 kg/m^3 per centimeter. Both the laminar and the turbulent regimes were examined, corresponding to $F = 0.4$, $Re = 600$ and $F = 6$, $Re = 9000$, respectively.

Two types of techniques were used to study the vortices, fluorescent-dye visualizations and conductivity measurements. In the fluorescent-dye visualizations, the dye was
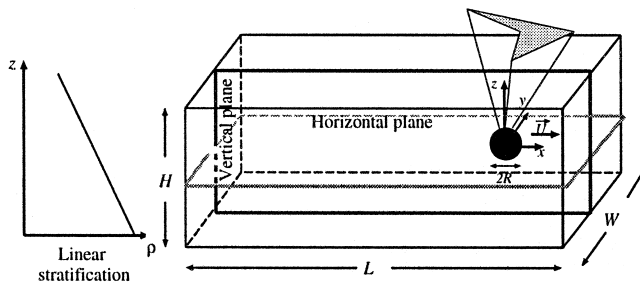

Fig. 1. Schematic diagram of the towing tank. The tank dimensions are $W = 0.8$ m, $H = 0.7$ m, $L = 7$ m. The usual linear stratification corresponds to a Brunt–Väisälä frequency close to one.

introduced into the fluid by painting the surface of the sphere. A horizontal laser-sheet is then used to illuminate the dye at the level of examination, thus revealing the presence and location of the vortices which are recorded on video tape. Conductivity measurements were performed using a four-electrode microscale conductivity probe manufactured by Precision Measurements Engineering (Head (1983)). The micro-conductivity probe is mounted within 1 mm of a fast-response thermistor which allows a correction of the density with regard to the local temperature in the tank. The noise level corresponds to about 10 g/m^3. The data were recorded at a rate of 200 Hz, and filtered at 100 Hz, which is below the limiting response of the thermistor. The temperature correction was required since the horizontal and vertical temperature variations naturally present in the tank are responsible for density deviations of the order of 1 kg/m^3.

The probe was used to measure two different types of profiles, vertical and horizontal.

2.1. Vertical profiles

In this configuration, the micro-conductivity probe was mounted on a vertical traverse fixed to the tank (Fig. 2(a)). The probe is first used to measure the background (linear) stratification before each tow, followed by a vertical scan through the core of a vortex structure. The fluid is allowed to settle at least 30 min after the sounding of the background stratification and 1 h before the next set of soundings. In order to assure that the vertical profiles were taken through the vortex cores, the vortices were simultaneously visualized with fluorescent-dye techniques (from the bottom of the tank). The conductivity probe typically scans 16 cm at 3 cm/s for the laminar regime, and 40 cm at 9 cm/s for the turbulent regime, which is fast enough to remain within the core of the structures given their advection speed. Such vertical scans thus provide a quasi-instantaneous density profile along the vertical direction of a single structure.

vertical profile configuration
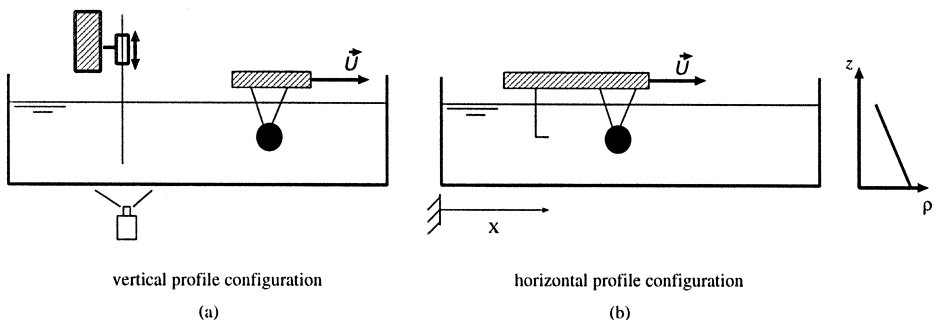(a)

horizontal profile configuration
(b)

Fig. 2. Experimental set-up for density measurements. (a) Vertical profile configuration: the probe is fixed with respect to the towing tank and is used to vertically traverse a single vortex at 3 cm/s in the laminar regime and 9 cm/s in the turbulent regime. The vortices are simultaneously visualized from the bottom of the tank to ensure that the traverse is taken through the core of the vortex. (b) Horizontal profiles configuration: the probe is fixed with respect to the moving sphere. Note that the probe position is defined in the reference frame of the tank ($\times$).

2.2. Horizontal profiles

In the second configuration, a L-shaped micro-conductivity probe was maintained at a fixed distance with respect to the sphere (Fig. 2(b)). The position of the probe is defined by the coordinate system (x, y, z) in the reference frame of the sphere (Fig. 1). The same kind of experimental sequence as for the vertical profiles was followed, i.e., the background (horizontal) density variations present in the tank were measured before those in the wake of the sphere. These horizontal density profiles were taken at several z-positions above and below the horizontal symmetry plane for one y-position ($y/R = 1$) corresponding to the cores of the positive side of the vortex street, and at several y-positions corresponding to two z-positions ($z/R = \pm 0.2$) where we measured the maximum density perturbation. Since the micro-conductivity probe is fixed with respect to the sphere, each measure is performed at a constant time $Nt(= (x/R)/\mathrm{F})$, and thus the resulting horizontal profiles provide truly instantaneous horizontal density profiles of the vortices. In order to represent the spatial dependence in these horizontal profiles, another streamwise coordinate (X) is introduced, which is fixed with respect to the tank (see Fig. 2(b)).

3. Balanced state of a single vortex

Earlier experiments using fluoresceine and a horizontal laser-sheet scanning the vertical direction revealed strong three-dimensional characteristics, with a finite vertical extent of the vortical structures (Bonnier et al. (1998)). Moreover, these vortices were found to be nearly circularly-shaped and to exhibit a very high degree of vertical coherence for a very long time. Here we wish to examine the role played by the density field in the internal dynamics of the vortex structures.

The interpretation of the stationary Boussinesq equations written in polar coordinates provides a first description of the balance of forces.

$$\begin{cases} \dfrac{u_\theta^2}{r} - \dfrac{1}{\rho_o} \dfrac{\partial p'}{\partial r} = 0 & \text{(a)} \\[2mm] \dfrac{1}{\rho_o} \dfrac{\partial p'}{\partial z} + \dfrac{g}{\rho_o} \rho' = 0 & \text{(b)} \end{cases}, \tag{1}$$

which implies

$$\frac{\partial}{\partial z}\left(\frac{u_\theta^2}{r}\right) + \frac{g}{\rho_o}\frac{\partial \rho'}{\partial r} = 0, \tag{2}$$

where p' and ρ' are the deviations of p and ρ with regard to the reference state $[p_o(z), \rho_o(z)]$ corresponding to the background stratification ($\rho = \rho_o + \rho'$, and $p = p_o + p'$). Eq. (1)(a) shows that the centrifugal force is balanced by the pressure gradient in the

horizontal direction and Eq. (1)(b) indicates the hydrostatic balance in the vertical direction. Given the finite vertical extent of the vortices, it is reasonable to suppose that a vertical velocity gradient exists since the azimuthal velocity component must vanish at some height. Such a vertical velocity gradient implies a vertical pressure gradient with a low pressure in the core through Eqs. (2) and (1)(b). The low pressure within the vortex core that would, on its own, have the effect of collapsing the structure, is vertically balanced by the ''stretching'' effect of the density field through buoyancy forces. Such ''stretching'' would occur if the upper part of the structure is lighter than the background stratification and the lower part is heavier. The horizontal and vertical balance of these forces is shown schematically in Fig. 3. The horizontal balance of centrifugal forces and pressure gradients is represented in Fig. 3(a) and the vertical hydrostatic balance is represented in Fig. 3(b). It should be remarked that in a purely two-dimensional situation, there is no vertical velocity gradient and therefore no effect on the background density.

On the basis of the visualization results, showing circularly-shaped vortices and vertical coherence, a simple analytical model is proposed to describe far-wake vortices. Each vortex is modelled as an isolated monopole with a Gaussian and z-dependent velocity field (Eq. (3)):

$$\begin{cases} u_r = 0 \\ u_\theta = \dfrac{Vr}{r_{max}} \exp \dfrac{1}{2} \left(1 - \dfrac{r^2}{r_{max}^2} - \dfrac{z^2}{z_{max}^2} \right). \\ u_z = 0 \end{cases} \tag{3}$$

The stationary Boussinesq equations in polar coordinates are used to derive the pressure and density fields. Integration of Eq. (1)(a) provides the expression for $p'(r, z)$ (Eq. (4))
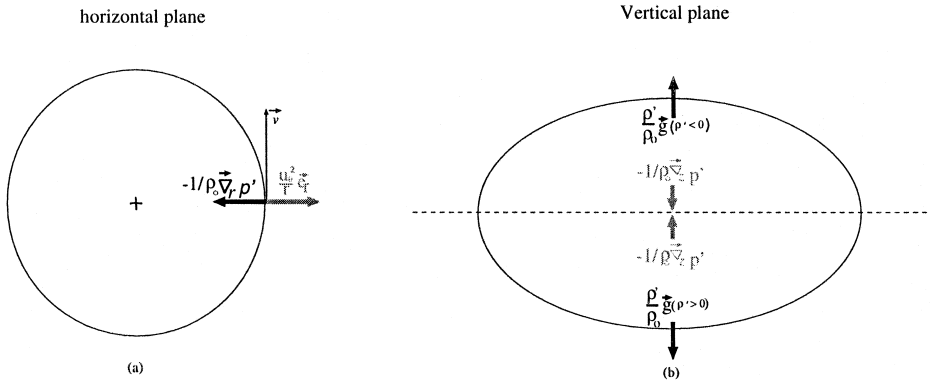

Fig. 3. Schematic view of the balanced state within a vortex structure. (a) Horizontal balance. (b) Vertical balance necessitating lighter fluid in the upper part of the vortex and heavier fluid in the lower part of the vortex.

showing that the vortex core corresponds to a pressure minimum. Then, using the vertical balance of Eq. (1)(b), the density field $\rho'(r,z)$ is calculated (Eq. (5)).

$$p'(r,z) = -\frac{\rho_o V^2}{2} \exp\left(1 - \frac{r^2}{r_{max}^2} - \frac{z^2}{z_{max}^2}\right) \tag{4}$$

$$\rho'(r,z) = -\frac{\rho_o V^2}{2} \frac{z}{z_{max}^2} \exp\left(1 - \frac{r^2}{r_{max}^2} - \frac{z^2}{z_{max}^2}\right) \tag{5}$$

The density isocontours in the vertical plane intersecting the vortex cores are shown in Fig. 4(a) for which we have set the aspect ratio z_{max}/r_{max} from our flow visualizations results. Fig. 4(b) is the associated horizontal profile $[\rho'(r)]$ at the z-level corresponding to the minimum of $\rho'(z)$ in the upper part of the vortex, while Fig. 4(c) corresponds to a vertical profile of the density deviation $\rho'(z)$ along the vertical axis in the vortex core. This density field illustrates how the density adapts to balance the
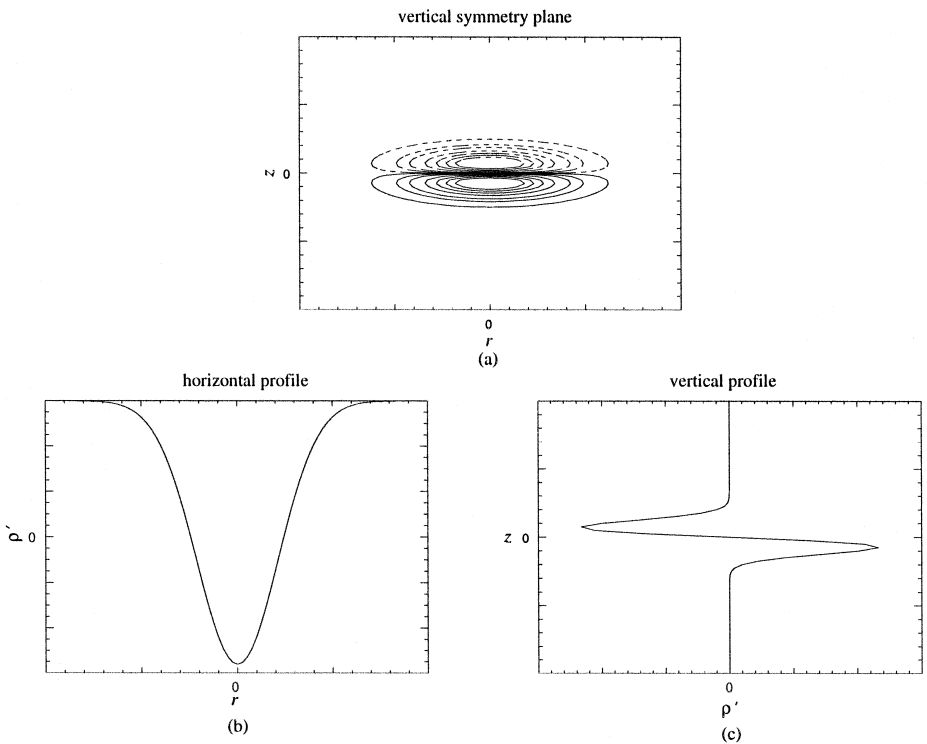

Fig. 4. Density deviation (ρ') of the idealized vortex. (a) Isocontours of $\rho'(r, z)$ in a vertical symmetry plane (dashed lines, negative values; solid lines, positive values). (b) Horizontal profile of $\rho'(r)$ at the z-level coinciding with the minimum density deviation in the upper part of the vortex. (c) Vertical profile of $\rho'(z)$ through the core of the vortex.

pressure drop in the vortex core via the hydrostatic balance. As can be seen in Fig. 4(a,c), the upper part of the vortex is lighter than the background stratification whereas the lower part is heavier, thus tending to counteract the pressure forces. The adaptation of the fluid to the hydrostatic balance is realized by the deformation of isopycnals. The presence of lighter fluid and heavier fluid with respect to the background stratification implies a pinching of the isopycnals, as shown in Fig. 5(a), corresponding to an intensification of the stratification (Fig. 5(b)).

The characterization of vortex structures by pinching of isopycnals also applies to geophysical applications, in the core of a cyclone, when rotation has to be taken into account. The flow in the present study verifies a horizontal centrifugal balance (Eq. (1)(a)) and a vertical hydrostatic balance (Eq. (1) (b)). In rotating systems, however, the geostrophic balance replaces the centrifugal balance in the horizontal direction, but in the vertical direction, the hydrostatic balance must still be verified. Thus, in the particular case of submeso-scale cyclonic vortices in the ocean, the low pressure in their core implies the same type of vertical adaptation of ρ' vs. p' to the hydrostatic balance. Of course, this would not be the case for anticyclonic submesoscale eddies, such as meddies or gulfstream rings, which are better documented and for which the ρ' vs. p' adaptation to the hydrostatic balance results in their well-known homogeneous core, observed, for example, by Armi et al. (1989).
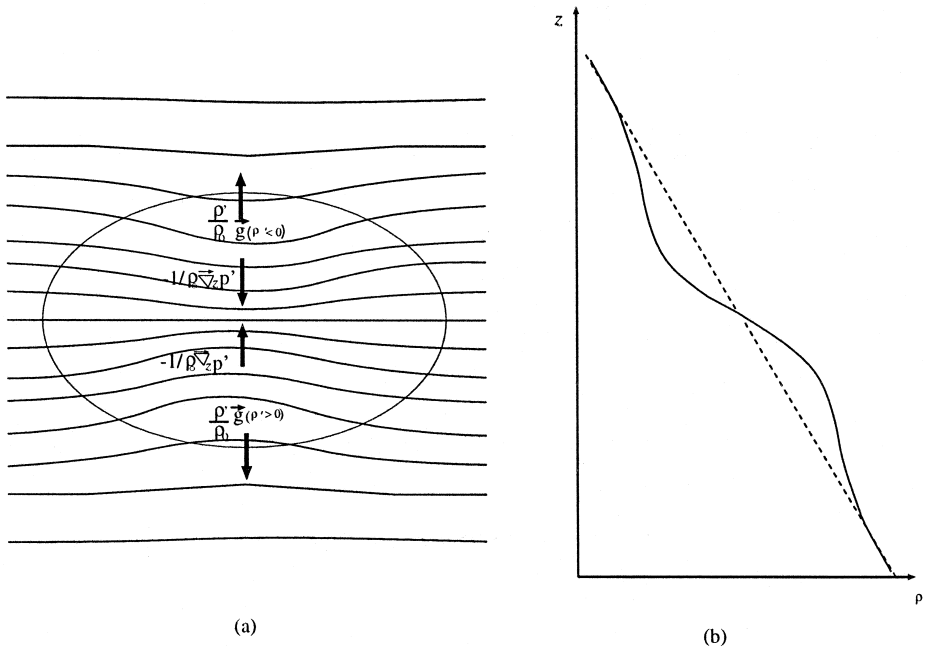

(a)

(b)

Fig. 5. (a) Deformation of the isopycnals in the vertical plane. The curvature adapts to allow hydrostatic balance. (b) Schematic diagram of the modification (intensification) of the density stratification in the core of the vortex (dashed line, background stratification).

4. Experimental results

Experiments have been performed for both the laminar ($F = 0.4$) and the turbulent ($F = 6$) regimes. For the laminar regime, horizontal profiles and vertical profiles of the density have been measured for dimensionless times between $Nt = 20$ and $Nt = 100$. Detailed results are presented for $Nt = 40$ in Sections 4.1.1 and 4.1.2 and the temporal evolution in Section 4.1.3. Results for the turbulent regime will be presented in Section 4.2.

The experimental data are usually presented in terms of the density deviation from the background density level, ρ'. This is achieved by subtracting the background density level (i.e., the unperturbed density level) measured prior to each run.

4.1. The laminar regime

4.1.1. Horizontal profiles

In this section, we will describe in detail the density field within the structure for $Nt = 40$. The vortices at that time have reached their evolved stage. Vortices in the early stages of their evolution will be discussed later in Section 4.1.3.

The horizontal density profiles were measured at a fixed distance (x) behind the sphere, for several y- and z-positions, thus providing a sequence of profiles through constant Nt vortices, i.e., vortices of the same age. In Fig. 6(a), the background horizontal density variations are superimposed with the density variations measured in the vortex street. The background density variations reveal a slight trend that can be attributed to a small maximum deviation in the horizontality of the towing system of about 1 mm. The corresponding deviation from the background stratification is plotted in Fig. 6(b). The initial non-periodic part of the signal measured in the vortex street corresponds to the beginning of the tow when no vortices are yet present at the probe location. After $X/D = 40$, the signals are very periodic with a frequency or Strouhal number ($St = fD/U = 0.20$) equivalent to the one found between adjacent vortices via flow visualizations. Nevertheless, it was still essential to determine the relative position of the density peaks with respect to the vortex cores. To this end, a two-step process was followed which was needed since the micro-conductivity probe cannot be used with particles necessary to obtain the vorticity field via PIV methods. The process consisted in synchronizing fluorescent-dye visualizations to the vorticity field and, separately, the fluorescent-dye visualizations to the density variations. In the first step, the maximum fluorescent-dye concentrations were shown to correspond to the peaks of maximum vertical vorticity, defining the vortex cores. In the second step, it was shown that the density peaks (maximum density deviations with respect to the background density level) coincide with the maximum dye concentration and thus with the cores of the vortices. Moreover, the density between two adjacent vortices of the same vortex street is unperturbed at the background density level. These results were confirmed for different dimensionless times ($Nt = 20, 35, 40$) and $z/R = \pm 0.2$. Typical results of the two-step process are shown in Fig. 7, where the simultaneously acquired vorticity field and fluorescent-dye visualizations (step 1) are superimposed with the horizontal density
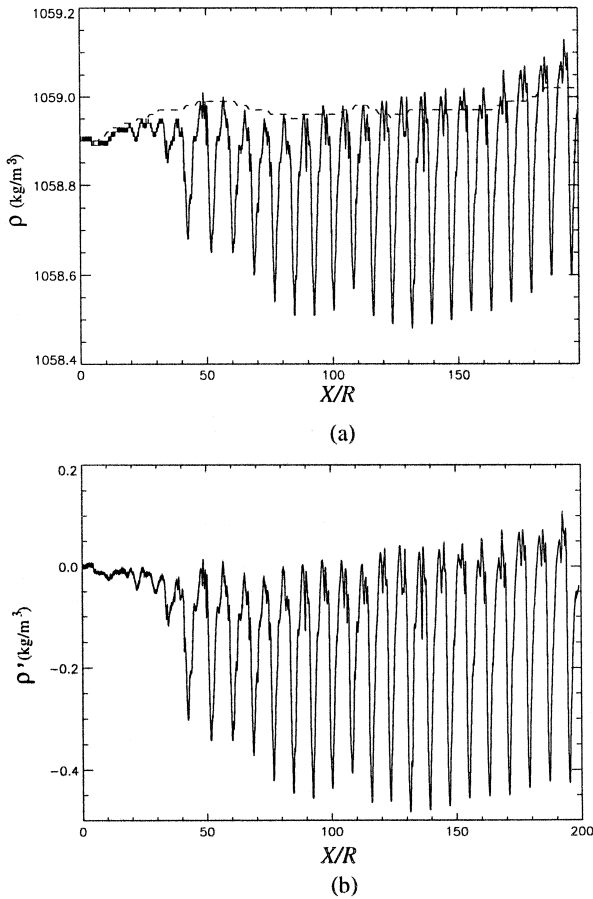
(a)

(b)

Fig. 6. Horizontal density variations along the axis of one vortex street at $F = 0.4$, $Nt = 40$ (probe location at $x/R = 16$, $y/R = 0.8$, $z/R = 0.2$). (a) Superposition of the density measured prior to the tow (dashed line), and the density recorded in the vortex street during the tow (solid line). (b) Difference of the two signals yielding the density deviation [$\rho'(X)$]. The initial portion of the signal corresponds to a region when no vortices are yet present at the probe location.

signal from step 2 performed through the cores of one side of the vortex street. It shows how the vorticity cores coincide with the density peaks.

The results of two simultaneously acquired horizontal density profiles, taken above and below the wake axis at $z/R = \pm 0.2$ are shown in Fig. 8. It can be seen that the density deviations are perfectly correlated above and below the wake axis with negative peaks above the wake axis and positive peaks below the axis, both associated with the cores of the vortices. This vertical coherence permits us to correlate different horizontal profiles taken separately at several z-positions, i.e., it allows us to construct vertical (z) profiles associated with the structure, and by inference transversal (y) profiles.

From two series of horizontal profiles in the x-direction, realized for different z-positions (at $y/R = 1$) and y-positions (at $z/R = 0.2$), a vertical mean profile and a

Fig. 7. Superposition of a simultaneously acquired fluorescent-dye visualization and vorticity isocontours computed from particle tracking with a density signal measured in the core of a vortex street at $F = 0.4$. The straight dotted line shows where the horizontal profile was performed. The sphere is moving from right to left.

transversal mean profile, respectively, were deduced. The average peak density deviations for each z-position and y-position were estimated over approximately 20 vortices, thus providing the instantaneous (i.e., $Nt =$ constant), vertical and transversal profiles shown in Fig. 9(a) and (b), respectively. The transversal profile exhibits a peak at $y/R = 1$ coinciding with the center of the vortex, as defined by the maximum ω_z-vorticity. It can be seen that the transversal profile is quite asymmetric, which is due to the presence of the opposite signed vortex street. While the location of this peak is not surprising, the vertical profile in Fig. 9(b) exhibits two density extrema of opposite sign,
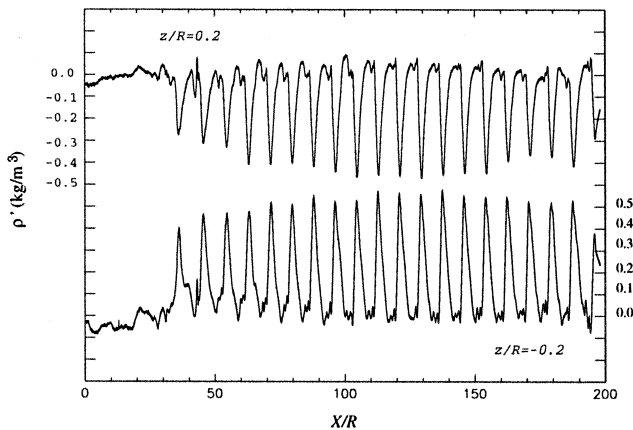

Fig. 8. Two simultaneously acquired density deviation profiles $[\rho'(X)]$ for $F = 0.4$, $Nt = 40$. The two probes are situated above and below the sphere axis at $x/R = 16$, $y/R = 0.8$ and $z/R = \pm 0.2$. The initial portion of the signal corresponds to a region when no vortices are yet present at the probe location.
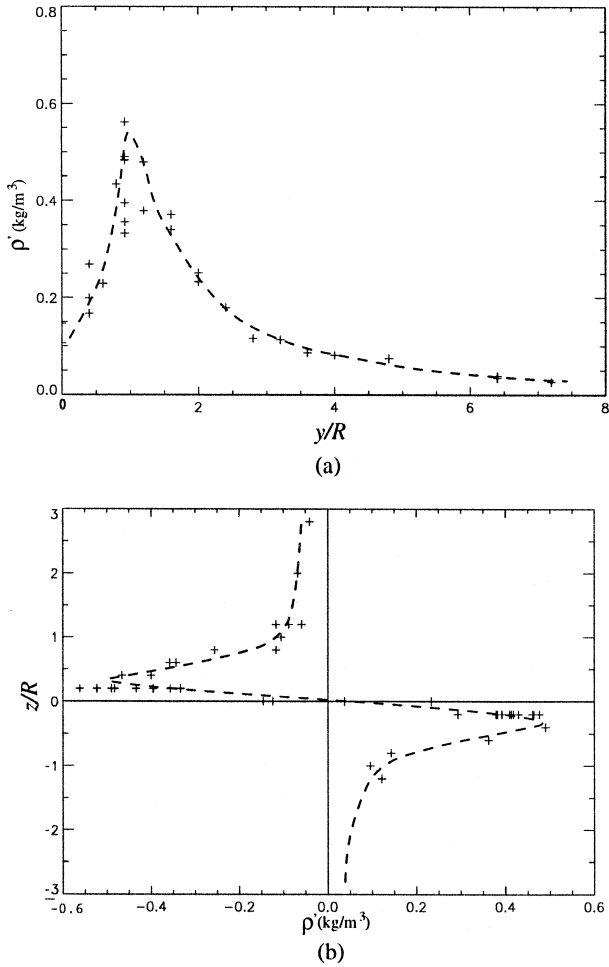
Fig. 9. Mean ρ' profiles inside a structure at $F = 0.4$, $Nt = 40$. (a) Mean horizontal profile of $\rho'(X)$ realized from a set of profiles at several y-positions, and for $x/R = 16$ and $z/R = 0.2$. (b) Mean vertical profile of $\rho'(z)$ realized from a set of profiles at several z-positions, and for $x/R = 16$ and $y/R = 1$.

above and below the wake axis at $z/R = \pm 0.2$. The two opposite signed extrema are closely spaced apart, resulting in a very abrupt change in the density deviation. On the wake axis, the density deviation is zero, implying that there is no mass transfer across the horizontal symmetry plane of the wake. Most importantly, the vertical profile in Fig. 9(b) is in good qualitative agreement with the theoretical profile in Fig. 4(c).

From these results, horizontal and vertical scales of the structures can be defined. Using a threshold of 10% of the maximum density deviation, yields an aspect ratio of the structure, H/L, of about 0.3. This scaling for far-wake vortices is in agreement with other vortices observed in freely decaying quasi-two-component turbulence such as

dipoles (e.g., Voropaev et al. (1991): $H/L = 0.29$ and Flór and Van Hejst (1996): $H/L = 0.34$), or for grid turbulence (e.g., Fincham et al. (1995): $H/L = 0.33$).

4.1.2. Vertical profiles

Although the vertical coherence of the vortices justifies the juxtaposition of the mean peak horizontal density deviations, the resulting vertical profiles only yield an average and discrete description of the density field within the vortex. Furthermore, in the turbulent regime, the vortices are too randomly distributed to allow such a juxtaposition. Thus direct vertical soundings were performed yielding quasi-instantaneous vertical density deviation profiles of *individual* structures.
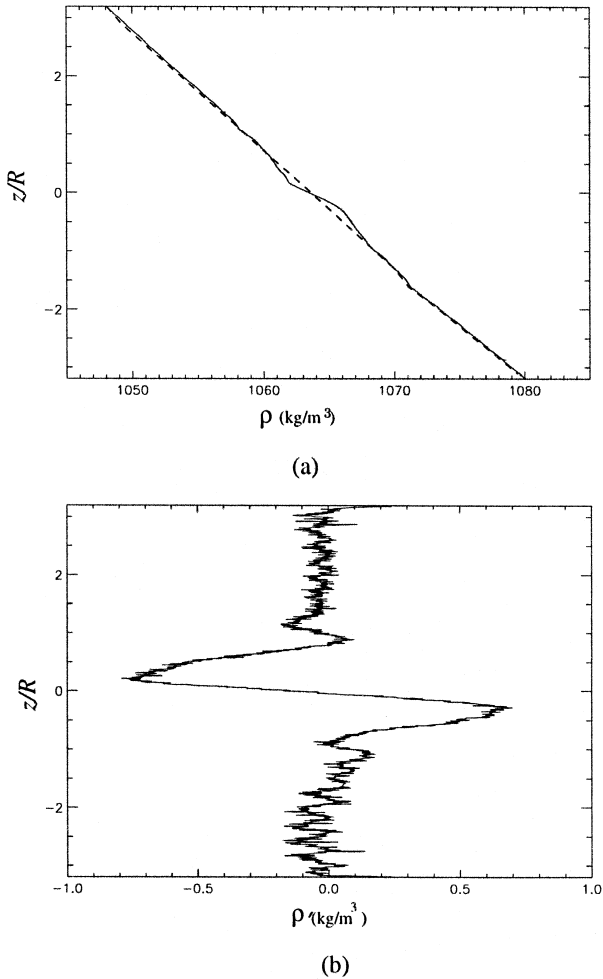

(a)

(b)

Fig. 10. Vertical density profiles within a structure at $F = 0.4$, $Nt = 40$. (a) Superposition of the background stratification measured prior to the tow (dashed line) and the density profile measured in the core of the structure (solid line). (b) Difference of the two signals yielding the density deviation [$\rho'(z)$].
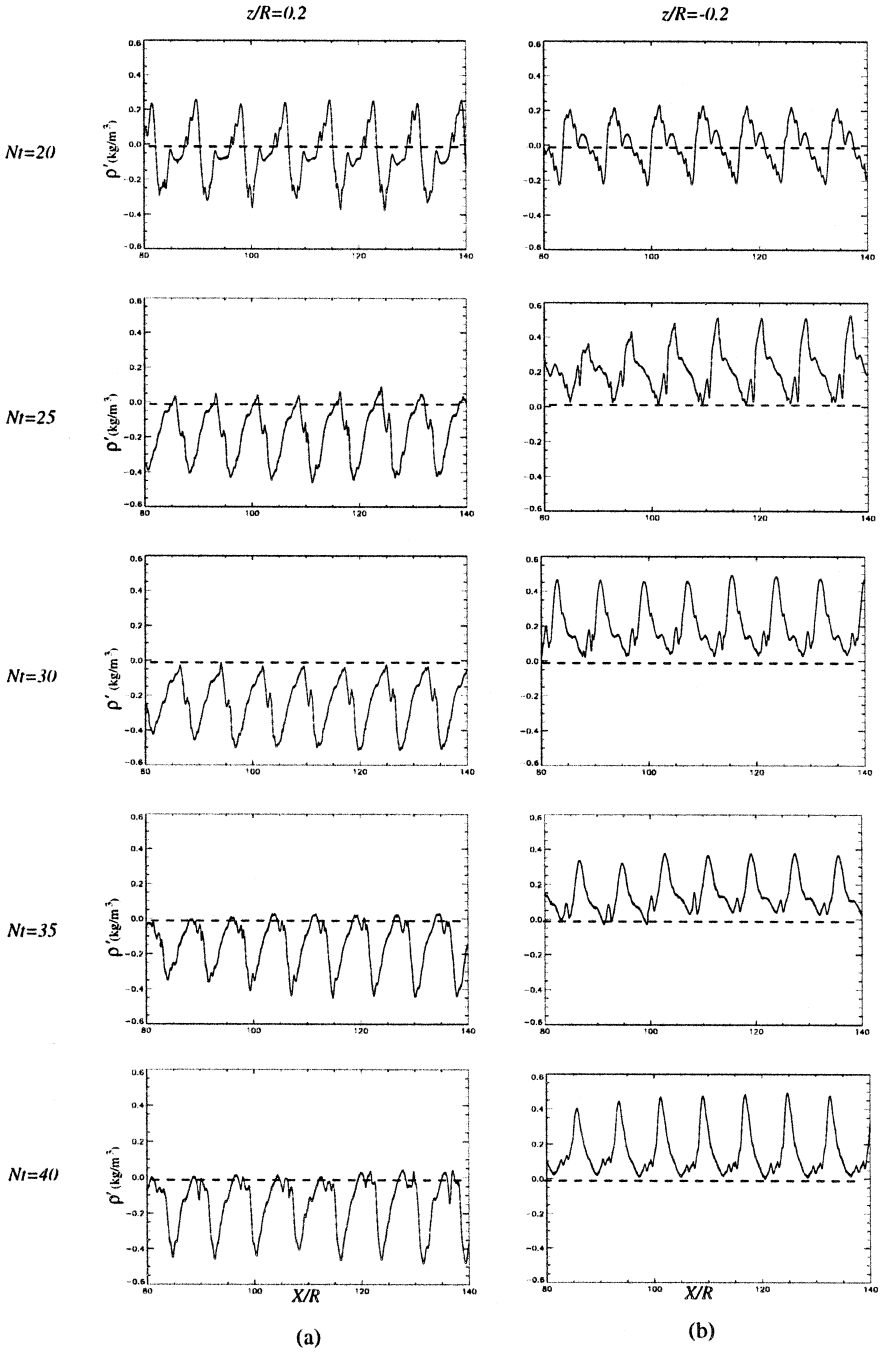
Fig. 11. Temporal evolution of horizontal profiles $\rho'(X)$ for $F = 0.4$ at $Nt = \{20, 25, 30, 35, 40\}$. (a) $z/R = 0.2$, (b) $z/R = -0.2$.
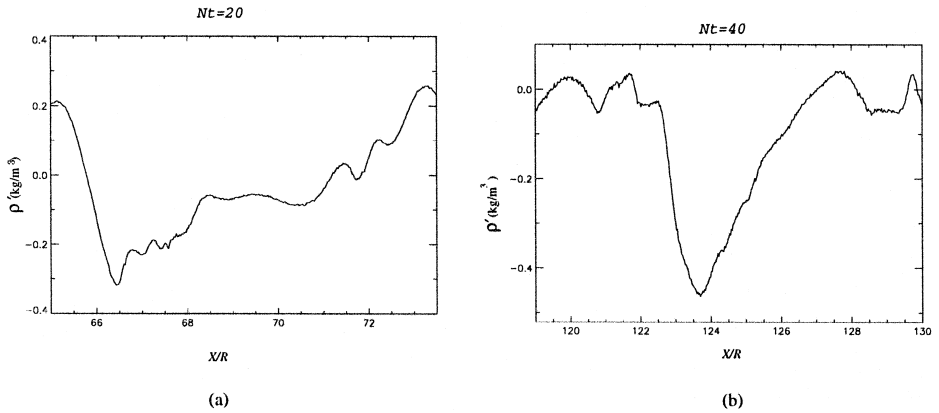
Fig. 12. Zoom of horizontal $\rho'(X)$ through a single vortex at $F = 0.4$ and $z/R = +0.2$. (a) $Nt = 20$, (b) $Nt = 40$. Data correspond to those shown in Fig. 11.

The vertical profiles in the laminar regime are measured by vertically traversing the vortex at a speed of 3 cm/s. This provides a quasi-instantaneous profile since the advection of the vortices during the traversing time ($N\Delta t = 6$) necesssary for the probe to scan the structure, is small compared to the evolution time, as seen later. As before, each run is preceded by a sounding of the background stratification. Fig. 10(a) shows a typical density profile within the structure superimposed with the background stratification. The corresponding deviation from the background stratification is plotted in Fig. 10(b). The profile is in good agreement with both the averaged vertical profile (Fig. 9(b)) deduced from the horizontal profiles, as well as the theoretical profile (Fig. 4(c)). The maximum density deviation is approximately $\rho'_{max} = 600$ g/m^3, corresponding for our stratification to a deflection of the isopycnal of $\Delta z = 0.5$ cm ($z/r = 0.2$).
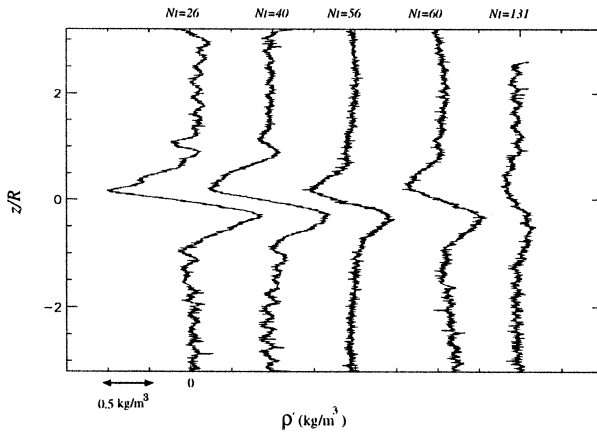

Fig. 13. Temporal evolution of the vertical $\rho'(z)$ profiles obtained for $Nt = \{26; 40; 56; 60; 131\}$ at $F = 0.4$ and at $y/R \in [0.8; 1.2]$. Each plot is shifted by 1 kg/m^3.

4.1.3. Temporal evolution

The temporal evolution for $Nt = \{20, 25, 30, 35, 40\}$ of the $\rho'(X)$-horizontal profiles is shown in Fig. 11(a,b) for $z/R = 0.2$ and $z/R = -0.2$, respectively. At $Nt = 20$, the profile is very asymmetric and the density deviation fluctuates evenly around the level of the background stratification, both the core of the vortices and the region between two adjacent vortices revealing an extremum of the density deviation. Very rapidly, however, the deviation between adjacent vortices relaxes whereas the deviation in the vortex cores themselves grows, and for increasing Nt, the peaks inside the vortices become more symmetric, resulting in smooth symmetric peaks for $Nt \geq 35$. This evolution of the horizontal density profile clearly shows that there exists a strong transitory regime up to $Nt = 35$, although $Nt = 20$ is usually seen as the time at which the far-wake can be considered to be characterized by mainly horizontal motions, i.e., having reached a quasi-steady state. If, however, the density profile is considered to be the determining parameter for characterizing the far-wake quasi-steady state, such a value for Nt should be closer to $Nt = 35$. For this reason the detailed examination of the profiles in Sections 4.1.1 and 4.1.2 was made at $Nt = 40$.

The symmetry of the density profile with respect to the background stratification at $Nt = 20$ is likely to be due to the initial process of vortex shedding and formation. In addition, not all experiments performed at $Nt = 20$ reveal such a clear symmetry with respect to the background stratification, which suggests that $Nt = 20$ corresponds to a zone of rapid transition.

To examine the asymmetry of the shape of the profiles, Fig. 12(a,b) shows a zoom on $\rho'(X)$ through a single vortex at $Nt = 20$ and $Nt = 40$. Fig. 12(a) shows that the density profile is much steeper on one side of the structure than on the other, i.e., the vortices at this early stage of formation exhibit a non-axisymmetric horizontal density structure. This is due to the fact that the structure is deformed by strong changes in upstream advection speed. At higher Nt, effects of advection become negligible and the vortex is more symmetric as shown in Fig. 12(b).

The temporal evolution was also examined via vertical soundings as presented in Fig. 13. The shape of the vertical profiles can be seen to be maintained up to at least
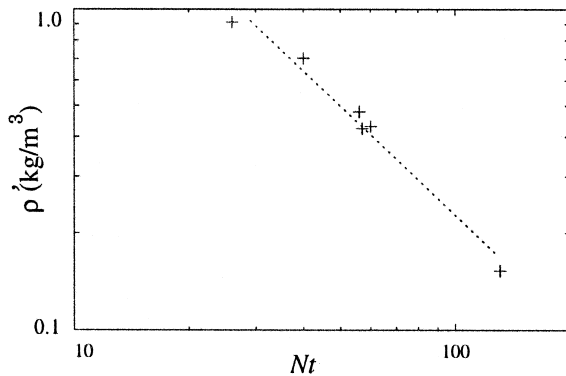

Fig. 14. Decay of the maximum density deviation in the core of a vortex for $F = 0.4$ at $y/R \in [0.8; 1.2]$. The dotted line is the best fit to the experimental data points and exhibits a -1.1 power law.

$Nt = 131$. The density deviation of the vortex core decays monotonically towards the background stratification, following a $(Nt)^{-1}$ power law as shown in Fig. 14. It should also be noted that the vertical density profiles do not show a detectable increase in the vortex height in the range investigated, which is consistent with the very slow vertical viscous growth found by Bonnier et al. (1998).

4.2. The turbulent regime

Since geophysical situations are concerned with high F and Re numbers, and since many features of the turbulent and laminar wakes are similar, the goal was to
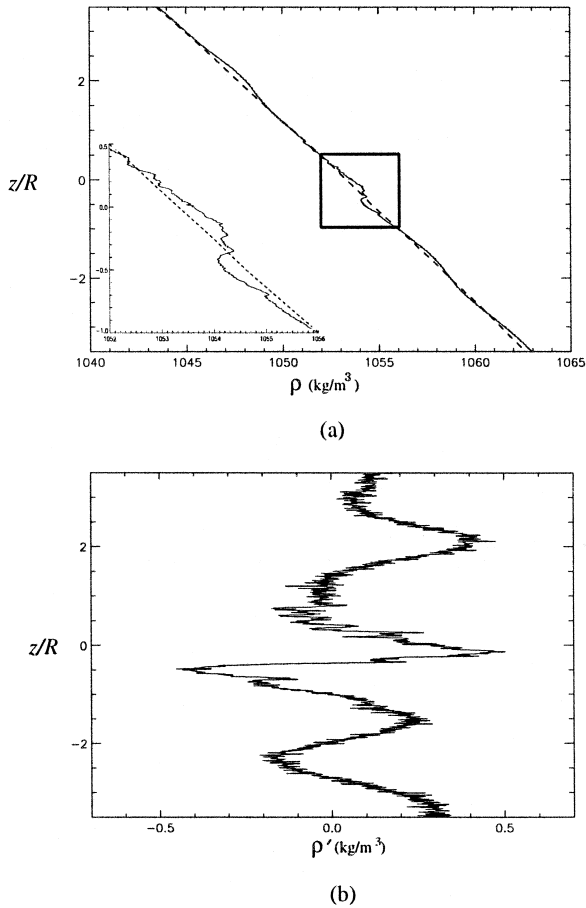

(a)

(b)

Fig. 15. Vertical profile within the turbulent wake at $F = 6$, $Nt = 10$ and $y/R = 1$. (a) Superposition of the background stratification measured prior to the tow (dashed line) with the density deviation $\rho'(z)$ measured in the core of the structure (solid line). A zoom of the region of interest is displayed in the left-hand corner of the graph. (b) Difference of the two signals yielding the density deviation $\rho'(z)$.

demonstrate whether or not the density field was also independent of the regime. In other words, can the structures just examined in the laminar regime also be found in the turbulent regime? To answer this question, vertical density soundings have been performed for the turbulent regime at $Nt = 10$ and $Nt = 40$. $Nt = 10$ corresponds to an early far-wake, after the three-dimensional near-wake has collapsed, but the vertical movements are still quite strong. At this stage, the wake is still undergoing strong mixing. The resulting vertical density profiles $\rho(z)$ and $\rho'(z)$, shown in Fig. 15(a) and (b), respectively, confirm a mixing by turbulent overturns, as expected from the three-dimensional movements still present at this stage. Such mixing events is what has been observed in other examples of the early stages of stratified turbulence (e.g., Voropaev et al., 1997) and is expected in any situation of strong mixing such as the near-wake itself. In the far-wake, however, the vertical density profile at $Nt = 40$ shown in Fig. 16 is found to be similar to the one measured in the laminar regime, i.e., exhibiting a local intensification of the background stratification. In terms of the density deviation, the profile (Fig. 15(a)) presents a density deviation in the opposite direction (Fig. 15(b)) of the one found in far-wake vortices (Fig. 16), i.e., a global homogenization of the ambient stratification. Locally, however, there are statically unstable layers suggesting that the fluid inside the turbulent wake is not fully homogenized but instead the density is reordered.

These results show that the evolution of the density profile undergoes a significant reversal. After first becoming globally homogenized due to the initial three-dimensional turbulence and mixing, the emergence of the far-wake vortices demands that the density profile restratifies, and stratifies stronger than the background stratification.

Although the examined turbulent regime has been described as a multi-layered regime by Chomaz et al. (1993), the experimental results revealed a density profile
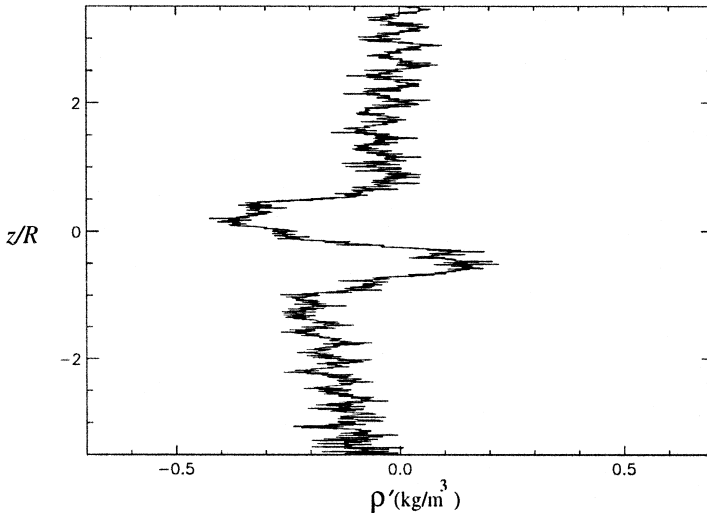

Fig. 16. Vertical profile of $\rho'(z)$ in the turbulent wake at $F = 6$, $Nt = 40$ and at $y/R = 0.8$.

characteristic of a single structure in the turbulent regime. Results in other turbulent wakes, e.g., Fincham et al. (1995) behind a rake of vertical bars showed that the flow is organized in several layers, each layer containing vortex structures. Although no evidence of such multilayers were found in the range of F and Re investigated, we would expect multi-layers to form at higher F and Re numbers and the described structures to be the building block of each layer.

5. Discussion and conclusion

The three dimensional internal density field of quasi two-component far-wake vortices generated by a sphere was described. It was experimentally shown that the core of the late vortices (as defined by an extremum of vertical vorticity), coincides with an intensification of the background stratification in both the laminar and turbulent regime. Specifically, a local minimum and maximum of density deviation was observed, respectively, above and below the sphere axis. This characterization of the vortex structures in terms of the density field is in good agreement with a proposed theoretical description of the balanced state of an isolated vortex structure. The isopycnals are deflected from their initial horizontal position to hydrostatically balance the pressure drop in the vortex core, resulting in an intensification of the background stratification. The temporal evolution of the intensified stratification is marked by a decay toward the background stratification.

Unlike the laminar regime, the turbulent regime is characterized by a globally homogenized near-wake. The transition between this initial state and the intensified stratification describes the collapse of the turbulent wake under the effect of the stratification. The initial wake fluid, mixed by the turbulence, contains available potential energy since it is unstable in its stratified surrounding due to the horizontal density gradients, which are a source of baroclinically generated motions. These motions will tend to flatten the fluid in the vertical direction and extend it in the horizontal direction, as first described by Schooley and Stewart (1963) in the case of a turbulent wake and by Wu (1969) in the case of an isolated (quiescent) mixed patch. During this gravitationally driven collapse, potential energy is transferred to kinetic energy, the fluid seeking to return to its initial density level. The resulting downward and upward motions toward the symmetry plane and a simultaneous outward motion, however, lead to an over-stratified state (a pinching of the isopycnals) in order to fulfill the requirement of the hydrostatic balance associated with the vortices. Only as the strength of the vortex decays, is the fluid allowed to come back to its original stratification.

Previous studies of the laminar and turbulent regimes suggested a strong qualitative resemblance for the vortices in the two regimes. For example, the decay of the peak vorticity (Spedding et al. (1996)) and the lateral spreading of the vortex street (Bonnier et al. (1998)) were found to have similar decay and growth rates in both regimes. The present study confirmed that the observed similarities between the two regimes are also found in terms of the density structure, confirming that the structure of the far-wake vortices is independent of the near-wake characteristics. The vortices in the turbulent

far-wake emerge from a globally homogenized state with vorticity present in the all three directions, whereas the vortices in the laminar regime are shed quasi two-dimensionally behind the sphere with a principal vertical vorticity component initiated by the flow passing around the sphere. This independence of the initial conditions suggests that the described internal density structure may be a general feature of quasi two-component vortices generated in stratified flows. This is certainly the case for a dipole generated by a turbulent jet (Fig. 17(a,b)), whose vertical density profile (Fig. 17(c)) taken through the core of one of the two head-vortices reveals the same characteristic profile as the ones performed in the wake vortices. (It should be noted that the vertical density measurements of Voropaev et al. (1991) in a dipole displayed a homogenized profile, since the measurements were performed during the initial period of dipole formation.) We therefore expect the internal density structure of all quasi two-component vortices found in stratified fluids to be the same. For example, preliminary examination of the underlying structures in multilayer flows strongly suggests the same density structures in each layer.
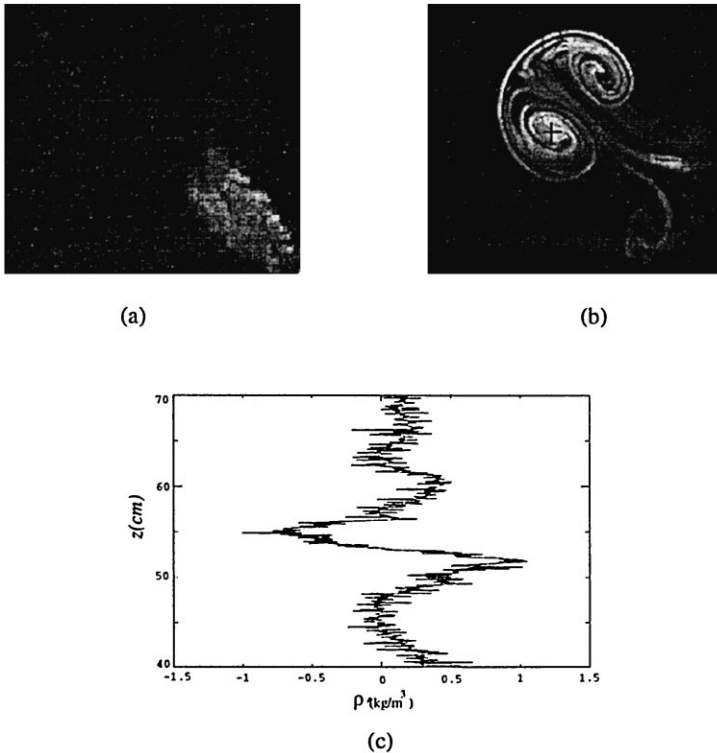

Fig. 17. Measurement of the density anomaly in a turbulent dipole. The dipole is generated by six micro-jets and is visualized using fluorescent dye. (a) Visualisation of the turbulent injected jet, (b) visualization of the dipole at $Nt = 40$, (c) vertical $\rho'(z)$ profile measured at $Nt = 42$. The $+$ symbol in (b) shows the position where the vertical density profile was performed.

Acknowledgements

References

Armi, L., Herbert, D., Oakey, N., Prince, J.F., Richardson, P.L., Rossby, H.T., Ruddik, B., 1989. Two years in the life of a Mediterranean salt lens. J. Phys. Oceanogr. 19, 354–370.

Bonnier, M., Bonneton, P., Eiff, O., 1998. Far-wake of a sphere in a stably stratified fluid: characterization of the vortex structures. Applied Scientific Research 59, 269–281.

Chomaz, J.M., Bonneton, P., Butet, A., Hopfinger, E.J., 1993. Vertical diffusion of the far wake of a sphere moving in a stratified fluid. Phys. Fluids 5 (11), 2799–2806.

Fincham, A., Maxworthy, T., Spedding, G.R., 1995. Energy dissipation and vortex structure in freely decaying stratified grid turbulence. Dyn. Atmos. Oceans 23, 155–169.

Flór, J.B., Van Hejst, G.J.F., 1996. Stable and unstable monopolar vortices in a stratified fluid. J. Fluid Mech. 311, 257–287.

Folkard, A.M., Davies, P.A., Fernando, H.J.S., 1997. Measurements in a turbulent patch in a rotating linearly-stratified fluid. Dyn. Atmos. Oceans 26, 27–51.

Fung, Y.T., Chang, S.W., 1996. Surface and internal wave signature of organized vortex motions in stratified fluids. Phys. Fluids 8 (11), 3023–3056.

Godeferd, F.S., Cambon, C., 1994. Detailed investigation of the energy transfers in homogeneous stratified turbulence. Phys. Fluids 6 (6), 2084–2100.

Head, M.J., 1983. The use of miniature four-electrode conductivity probes for high resolution measurements of turbulent density or temperature variations in salt-stratified water flows. PhD Thesis, Univ. of California, San Diego, CA.

Lin, Q., Boyer, D.L., Fernando, H.J.S., 1992. Turbulent wakes of linearly stratified flow past a sphere. Phys. Fluids 4 (8), 1687–1696.

McWilliams, J.C., 1985. Submesoscale coherent vortices in the ocean. Rev. Geophys. 23 (2), 165–182.

Riley, J.J., Metcalfe, R.W., Weissman, M.A., 1981. Direct numerical simulations of homogeneous turbulence in density-stratified fluids. In: West, B.J. (Ed.), Proc. AIP Conf. Nonlinear Properties of Internal Waves, pp. 79–112.

Schooley, A., Stewart, R.W., 1963. Experiments with a self propelled body submerged in a fluid with a vertical density gradient. J. Fluid Mech. 15, 83–96.

Spedding, G.R., Browand, F.K., Fincham, A.M., 1996. Turbulence, similarity scaling and vortex geometry in the wake of a towed sphere in a stably stratified fluid. J. Fluid Mech. 314, 53–103.

Voropaev, S.I., Afanasyev, Y.D., Filippov, I.A., 1991. Horizontal jet and vortex dipoles in a stratified fluid. J. Fluid Mech. 227, 543–566.

Voropaev, S.I., Xiuzhang, Z., Boyer, D.L., Fernando, H.J.S., Pok, C.-W., 1997. Horizontal jets in a rotating stratified fluid. Phys. Fluid 9 (1), 115–126.

Wu, J., 1969. Mixed region collapse with internal wave generation in a density-stratified medium. J. Fluid Mech. 35, 531–544.